Inorganic Chemistry

Article

pubs.acs.org/IC

Detection of Nitric Oxide and Nitroxyl with Benzoresorufin-Based Fluorescent Sensors

Ulf-Peter Apfel,[†] Daniela Buccella,[†,‡] Justin J. Wilson,[†] and Stephen J. Lippard*[,†]

[†]Department of Chemistry, Massachusetts Institute of Technology, Cambridge, Massachusetts 02139, United States

[‡]Department of Chemistry, New York University, New York, New York 10003, United States

Supporting Information

ABSTRACT: A new family of benzoresorufin-based copper complexes for fluorescence detection of NO and HNO is reported. The copper complexes, CuBRNO1−3, elicit 1.5−4.8-fold emission enhancement in response to NO and HNO. The three sensors differ in the nature of the metal-binding site. The photophysical properties of these sensors are investigated with assistance from density functional theory calculations. The fluorescence turn-on observed upon reaction with HNO is an unexpected result that is discussed in detail. The utility of the new sensors for detecting HNO and NO in HeLa cells and RAW 264.7 macrophages is demonstrated.

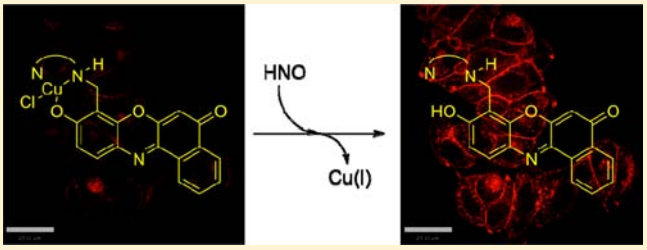

INTRODUCTION

Reactive nitrogen (RNS) and oxygen species (ROS) have numerous biological consequences.[1] Among these species, nitric oxide (NO), initially identified as an endothelial-derived relaxation factor,[2] has a broad variety of biological regulatory and signaling functions.[3−8] Biological NO is generated by oxidation of L-arginine to L-citruline by a class of enzymes known as nitric oxide synthases (NOS).[9] Among its many functions, NO plays important roles in the control of smooth muscle relaxation and vasodilation,[10] platelet aggregation in vascular endothelial cells,[11] neurotransmission,[12] and regulation of the immune response by macrophages.[13] Recently, it was suggested that nitroxyl (HNO), the one-electron-reduced congener of NO, is formed by NOS via oxidative degradation of L-arginine.[14,15] Some recent in vitro studies using HNO-releasing molecules demonstrated that HNO increases the contractility of heart cells,[16] leads to vasorelaxation in muscle cells,[17] and decreases platelet aggregation.[18] Taken together, these findings suggest that HNO also plays a pivotal role in biology.

In order to advance our insight into the physiological and pathological roles of HNO and NO, our group has focused on designing fluorescent sensors that selectively respond to these small molecules and afford both spatial and temporal information regarding the natural occurrence of these species at the cellular level. Various NO sensors, including *o*-diaminofluorescein, *o*-diaminonaphthalene, *o*-diaminocyanine,[19−21] luminescent lanthanide complexes,[22] and 5-amino-1-naphthonitrile (NO550),[23] detect NO in the presence of oxygen. Sensors for HNO include metalloporphyrins,[24] thiols,[25] and phosphines.[26] In contrast to these reagents, copper-based fluorescent probes like CuFL1,[27,28] CuFL2E,[29] and CuSNFL[30] developed by our group (Scheme 1) and others[31,32] provide direct, selective, and fast detection of NO both in vitro and in vivo. We have also recently described a selective HNO sensor, CuBOT1.[33,34] The emission intensity of these copper-based sensors is modulated by the oxidation state of the copper ion, which, in turn, can be modified by the RNS of interest. The CuFL and CuSNFL sensors react with NO to form the emissive nitrosamines FL-NO and SNFL-NO, with concomitant formation of Cu^{I} ions that dissociate from the complex.[30,35] The copper complex CuBOT1, on the other hand, reacts selectively with HNO, leading to reduction of the paramagnetic Cu^{II} ion and fluorescence enhancement.[33] The different reactivity of CuBOT1 versus CuFL and CuSNFL presumably arises from the lack of a secondary amine in the

Scheme 1. Small-Molecule Metal-Containing Sensors for NO (Cu[FL1]) and HNO (Cu[BOT1]) as Well as Their Reactions with Analytes[30,33]

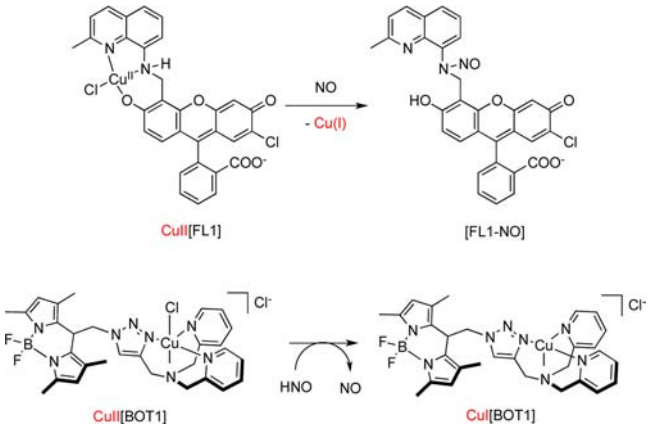

Received: December 19, 2012
Published: March 5, 2013

   dx.doi.org/10.1021/ic302793w | *Inorg. Chem.* 2013, 52, 3285−3294

former, which is the preferred site of attack on CuFL by NO.[35] A limitation of both fluorescein- and BODIPY-based sensors is their high-energy absorption and emission as well as their moderate Stokes shifts of about 30 nm. These features can cause problems associated with light scattering, which may lead to a low signal-to-noise ratio. Additionally, for biological imaging purposes, it is desirable to have sensors that emit far into the red, because low-energy radiation penetrates tissue more effectively.

In our continuing efforts to design improved sensors for NO and HNO, we have functionalized a benzoresorufin fluorophore with a Cu-binding site that contains a secondary amine, and we investigated its ability to detect ROS and RNS. Resorufin dyes emit at wavelengths >600 nm with Stokes shifts up to 60 nm.[36] Accordingly, sensors based on resorufin dyes should exhibit less background absorption and emission from biological samples and provide an advantage over previously reported green emitters in terms of tissue penetration depth. The synthesis and characterization of three benzoresorufin-based sensors are described herein. As with our previous systems, the Cu^{II}/Cu^{I} redox couple is used to modulate the emission response of the sensors to NO and HNO. Despite the availability of a secondary amine, a potential site of attack of NO, we found that the benzoresorufin-based probes show a better turn-on response for HNO than for NO.

MATERIALS AND METHODS

Synthetic Materials and Methods. All reactions were carried out under an N_2 atmosphere using standard Schlenk techniques. ^1H and $^{13}C\{^1H\}$ NMR spectra were recorded with a Varian Mercury 300 NMR or a Varian Inova 500 NMR spectrometer at room temperature. Peaks were referenced to residual ^1H signals from the deuterated solvent and are reported in parts per million (ppm). 2-Methyl-4-nitrosoresorcinol was synthesized by a literature procedure.[37] All other compounds were obtained from commercial vendors and used without further purification. Mass spectra were obtained with either an Agilent 5973 Network mass-selective detector connected to an Agilent 689N Network GC system or an Agilent 1100 Series LC/MSA trap. High-resolution mass spectral analyses were carried out at the Massachusetts Institute of Technology (MIT) Department of Chemistry Instrumentation Facility (DCIF). UV−vis spectra were recorded with a Varian Cary 1E spectrometer at 25 °C. Fluorescence spectra were obtained on a Quanta Master 4 L-format scanning spectrofluorimeter (Photon Technology International) at 25 or 37 °C. X-band electron paramagnetic resonance (EPR) spectra were collected with a Bruker EMX spectrometer equipped with an ER4199HS cavity and a Gunn diode microwave source. All solvents were dried prior to use according to standard methods. Silica gel 60 321 (0.015−0.040 mm) was used for column chromatography. Thin-layer chromatography was performed using Merck TLC aluminum sheets, silica gel 60 F254.

9-Hydroxy-8-methyl-5-benzo[*a*]phenoxazone (1). 2-Methyl-4-nitrosoresorcinol (1.31 g, 7.68 mmol) and 1,3-dihydroxynaphthalene (1.23 g, 7.68 mmol) were dissolved in *n*-butanol (20 mL) and heated to 50 °C. To this solution was added concentrated sulfuric acid (2.6 mL), and the mixture was stirred for 15 min at 50 °C. The mixture was allowed to cool to room temperature, and after 12 h, a dark precipitate formed. The precipitate was collected by filtration, washed with a mixture of ethanol and *n*-butanol (1:1, 10 mL) and then water/ethanol (1:1, 50 mL), and dried under vacuum. This material (2.11 g, 96% yield) was used without further purification. ESI-MS. Calcd for $[C_{17}H_{11}NO_3]^-$: 277.1. Found: 277.0.

8-Methyl-5-oxo-benzo[*a*]phenoxazin-9-yl acetate (2). Compound **1** (1.41 g, 5.09 mmol) was dissolved in acetic anhydride (20 mL) and pyridine (2 mL). The mixture was heated for 3 h at 100 °C and then left to stand at room temperature for 24 h. The resulting dark-red crystalline solid was collected by filtration and washed with a small amount of acetic anhydride and then a large volume of water. The solid was dried under vacuum, yielding 1.06 g (65%) of an orange crystalline material. ^1H NMR ($CDCl_3$, 300 MHz, ppm): δ 8.71−8.67 (1H, m), 8.30−8.27 (1H, m), 7.78−7.73 (2H, m), 7.68 (1H, d, ^3J = 9 Hz), 7.07 (1H, d, ^3J = 9 Hz), 6.46 (1H, s), 2.39 (3H, s), 2.27 (3H, s). ^{13}C NMR ($CDCl_3$, 75 MHz, ppm): δ 184.1, 169.0, 151.2, 149.8, 132.4, 132.3, 132.0, 131.4, 130.9, 130.2, 127.8, 126.1, 124.9, 119.2, 118.8, 117.1, 107.7, 21.0, 9.1. ESI-MS. Calcd for $[C_{19}H_{13}NO_4 + H^+]^+$ 320.1. Found: 320.2. Mp: 234−235 °C.

6-Bromo-8-bromomethyl-5-oxo-benzo[*a*]phenoxazin-9-yl acetate (3). Compound **2** (2.62 g, 8.2 mmol), 1,3-dibromo-5,5′-dimethylhydantoin (5.16 g, 0.018 mol), and VAZO88 (0.72 g, 3.0 mmol) were dissolved in dry chlorobenzene (300 mL) under an N_2 atmosphere. Acetic acid (700 μL) was added, and the solution was heated at 60 °C until ^1H NMR spectroscopy revealed full conversion to the final molecule (6−10 days). The hot solution was then washed with hot water (60 °C, 2 × 50 mL) and brine (100 mL) and dried with sodium sulfate. Evaporation of the organic fractions to dryness afforded an orange solid, which was washed with diethyl ether/pentane (1:1). The solid was collected by filtration and dried under vacuum to afford 3.6 g (92%) of an orange solid. ^1H NMR ($CDCl_3$, 300 MHz, ppm): δ 8.71−8.69 (1H, m), 8.38−8.35 (1H, m), 7.86−7.76 (3H, m), 7.26−7.23 (1H, m), 4.73 (2H, s), 2.46 (3H, s). ESI-MS. Calcd for $[C_{19}H_{11}Br_2NO_4 + Na^+]^+$: 497.9. Found: 497.8. Mp: 221 °C.

6-Bromo-8-formyl-9-hydroxy-5-benzo[*a*]phenoxazone (4). Compound **3** (1.5 g, 3.16 mmol) and sodium bicarbonate (1.8 g, 21 mmol) were dissolved in dimethyl sulfoxide (DMSO; 50 mL) and heated at 150 °C for 2 h. After cooling to room temperature, the blue solution was poured into 300 mL of HCl (4 M), and the resulting mixture was stirred for 1 h. The obtained brown precipitate was collected by filtration, washed with water, and dried under vacuum. The crude material was purified by silica gel column chromatography (dichloromethane to dichloromethane/methanol 100:2). The obtained residue was washed with 20 mL of diethyl ether/pentane (1:1) to afford 382 mg (29%) of a dark-orange solid. ^1H NMR ($CDCl_3$, 300 MHz, ppm): δ 12.10 (1H, s), 10.71 (1H, s), 8.70−8.67 (1H, m), 8.40−8.37 (1H, m), 8.01 (1H, d, ^3J = 9 Hz), 7.85−7.74 (2H, m), 7.02 (1H, d, ^3J = 9 Hz). ESI-MS. Calcd for $[C_{17}H_8BrNO_4+H^+]^+$: 370.0. Found: 369.9. Mp: 254 °C.

6-Bromo-9-hydroxy-8-[[(2-methylquinolin-8-yl)amino]-methyl]-5-benzo[*a*]phenoxazone (BRNO1). Compound **4** (25 mg, 0.068 mmol) and 8-amino-2-methyl-quinoline (11 mg, 0.07 mmol) were dissolved in dry methanol (10 mL) and stirred at room temperature for 1 h. The solution was cooled to 0 °C, and sodium cyanoborohydride (102 mg, 1.62 mmol) was added in one portion. The mixture was stirred for 36 h at room temperature and then poured into 10 mL of aqueous 5 M HCl. The resulting precipitate was filtered off and washed with copious amounts of water and then dichloromethane/hexane (10 mL, 1:1). Subsequently, the solid was dried under vacuum to afford 14.2 mg (41%) of a dark-red compound. ^1H NMR (CD_3OD, 500 MHz, ppm): δ 12.33 (1H, s), 9.41 (1H, d, ^3J = 6 Hz), 9.03 (1H, d, ^3J = 6 Hz), 8.95−8.91 (1H,m), 8.71−8.68 (1H, m), 8.64−8.61 (1H, m), 8.55 (1H, d, ^3J = 6 Hz), 8.20 (1H, d, ^3J = 6 Hz), 8.14−8.11 (1H, m), 7.95 (1H, d, ^3J = 6 Hz), 7.90 (1H, d, ^3J = 6 Hz), 7.87 (1H, d, ^3J = 6 Hz), 5.59 (2H, s), 3.46 (3H, s). ESI-HRMS. Calcd for $[C_{27}H_{18}N_3BrO_3 - H^+]^-$: 510.0453. Found: 510.0439. Mp: 184 °C (dec).

6-Bromo-9-hydroxy-8-[(quinolin-8-ylamino)methyl]-5-benzo[*a*]phenoxazone (BRNO2). Compound **4** (20 mg, 0.054 mmol) and 8-aminoquinoline (9.4 mg, 0.065 mmol) were dissolved in dry methanol (10 mL) and stirred at room temperature for 2 h. The solution was then cooled to 0 °C, and sodium cyanoborohydride (50 mg, 0.79 mmol) was added in one portion. The mixture was stirred for 72 h at room temperature and poured into a 20 mL solution of a saturated aqueous sodium bicarbonate solution. The resulting precipitate was filtered off and washed with water. Drying under vacuum afforded 10.6 mg (39%) of a dark-purple solid. ^1H NMR (DMSO-d_6, 500 MHz, ppm): δ 8.70 (1H, d, ^3J = 6 Hz), 8.57 (1H, d, ^3J = 6 Hz), 8.22 (1H, d, ^3J = 6 Hz), 8.18 (1H, d, ^3J = 6 Hz), 7.83−7.80 (1H, m), 7.72−7.69 (1H, m), 7.61 (1H, d, ^3J = 6 Hz), 7.48−7.44 (1H, m), 7.36−7.33 (1H, m), 7.17 (1H, d, ^3J = 6 Hz), 7.05 (1H, d, ^3J = 6

dx.doi.org/10.1021/ic302793w | Inorg. Chem. 2013, 52, 3285−3294

Hz), 6.83 (1H, d, ^3J = 6 Hz), 4.73 (2H, s), 2.62 (3H, s). ESI-HRMS. Calcd for $[C_{26}H_{16}N_3BrO_3 - H^+]^-$: 496.0297. Found: 496.0293. Mp: 256 °C (dec).

6-Bromo-9-hydroxy-8-[[(pyridin-2-ylmethyl]amino]methyl)-5-benzo[*a*]phenoxazone (BRNO3). Compound **4** (20 mg, 0.054 mmol) and 2-(aminomethyl)pyridine (11 μL, 0.11 mmol) were dissolved in dry methanol (5 mL), and the resulting solution was stirred at room temperature for 1 h. The solution was then cooled to 0 °C, and sodium cyanoborohydride (66 mg, 0.10 mmol) was added in one portion. The mixture was stirred for 48 h at room temperature, and a saturated aqueous solution of sodium bicarbonate (20 mL) was added. The resulting precipitate was filtered off, washed with water (10 mL), and dried under vacuum to afford 21.4 mg (43%) of a purple solid. ^{1}H NMR (CD_3OD, 500 MHz, ppm): δ 8.72 (1H, d, ^3J = 6 Hz), 8.41 (1H, d, ^3J = 6 Hz), 8.34 (1H, d, ^3J = 6 Hz), 7.78–7.73 (2H, m), 7.67–7.63 (1H, m), 7.60 (1H, d, ^3J = 6 Hz), 7.51 (1H, d, ^3J = 6 Hz), 7.25–7.24 (1H, m), 6.79 (1H, d, ^3J = 6 Hz), 4.23 (2H, s), 4.03 (2H, s). ESI-HRMS. Calcd for $[C_{23}H_{16}N_3BrO_3 - H^+]^-$: 460.0297. Found: 460.0293. Mp: 256 °C (dec).

Headspace EI-MS Studies. BRNO1 (0.95 mg, 1.86 μmol) was dissolved in acetonitrile (1 mL), and 0.8 equiv of $CuCl_2·2H_2O$ (0.2 mg, 1.18 μmol, in 1 mL acetonitrile) was added to this solution in a custom-made, gastight cell in an inert-atmosphere glovebox. The mixture was maintained at room temperature for 1 h, prior to addition of 10 mg of Angeli's salt. The cell was connected to a He gas-flow inlet tube and to the mass spectrometer. The connecting copper tubing was purged thoroughly with He prior to analysis of the reaction headspace. Headspace analysis was performed with the mass spectrometer operating in selective ion mode.

Cyclic Voltammetry. Cyclic voltammograms were measured in a three-electrode cell with a 2.0-mm-diameter glassy carbon working electrode, a platinum auxiliary electrode, and a $Ag/AgNO_3$ reference electrode in acetonitrile. The solvent contained *n*-$Bu_4N(PF_6)$ (0.05 M) as the supporting electrolyte. The measurements were performed at room temperature with a VersaSTAT3 (AMETEK) galvanostat. Deoxygenation of the samples was accomplished by passing a stream of N_2 through the solutions for 5 min prior to the measurements, and the solutions were kept under N_2 for the duration of the study. All data were referenced to the Fc/Fc^+ couple as an internal standard ($E_{1/2}$ = +405 mV vs $Ag/AgNO_3$ reference electrode).

X-ray Data Collection and Structure Solution Refinement. Crystals of **2** and **3** were grown by slow evaporation of solutions of the compounds dissolved in chloroform. Single crystals suitable for X-ray analysis were coated with Paratone-N oil, mounted on a fiber loop, and placed in a cold, gaseous N_2 stream on a Bruker APEX CCD X-ray diffractometer performing φ and ω scans at 100(2) K. Diffraction intensities were measured using graphite-monochromated Mo Kα radiation (λ = 0.71073 Å). Data collection, indexing, initial cell refinements, frame integration, and final cell refinements were accomplished with the program *APEX2*.[38] Absorption corrections were applied using the program *SADABS*.[39] The structure was solved by direct methods using *SHELXS*[40] and refined against F^2 on all data by full-matrix least squares with *SHELXL-97*[41] following established refinement strategies. Crystallographic data collection and refinement parameters are presented in Tables S1 and S2 in the Supporting Information (SI).

Density Functional Theory (DFT) Calculations. All calculations were performed with the *Gaussian 03* program package[42] using the B3LYP functional.[43,44] Geometry optimizations were carried out in the gas phase using the 6-31g(d,p) basis set.[45] Frequency calculations were carried out at the same level of theory to ensure that geometries converged to true local minima on the potential energy surface. The 30 lowest-energy singlet excited states were computed with time-dependent DFT (TDDFT) calculations. For these calculations, the larger 6-311++g(d,p) basis set was utilized. Solvent effects were modeled with the conductor-like polarizable continuum model for water.[46] Electron-density difference maps (EDDMs) and calculated UV–vis absorbance spectra were generated with the program *GaussSum2.2*.[47] Tables S3–S12 in the SI contain the coordinates of optimized structures and a summary of the lowest-energy singlet excited states.

Spectroscopic Materials and Methods. Piperazine-*N*,*N*′-bis(2-ethanesulfonic acid) (PIPES; Calbiochem) and potassium chloride (99.999%, Aldrich) were used to prepare buffered solutions (50 mM PIPES, 100 mM KCl, pH 7.0) in deionized water with resistivity ≥18 MΩ cm^{-1}, obtained using a Milli-Q water purification system. Nitric oxide (NO) was purchased from Airgas and purified as previously described.[48] *S*-Nitroso-*N*-acetylpenicillamine (SNAP), *S*-nitroso-L-glutathione (GSNO), sodium peroxynitrite, and Angeli's salt were purchased from Cayman Chemical and stored at −80 °C when not in use. NO and the other RNS were injected into buffered solutions via a gastight syringe. $CuCl_2·2H_2O$ (99+%, Alfa Aesar) was used to prepare 7 mM $CuCl_2$ stock solutions in DMSO. Dye stock solutions were prepared in DMSO (5 mmol/L) and stored at −80 °C when not in use. Measurements were performed under inert-atmosphere conditions. Quantum yields of BRNO1–3 were determined in 50 mM PIPES buffer (100 mM KCl, pH 7) using resorufin (λ_{em} = 585 nm, λ_{ex} = 572 nm, and Φ = 0.74[49]) as the reference in water (pH 9.5).

Cell Culture. HeLa cells and Raw 264.7 murine macrophages were cultured in Dulbecco's modified Eagle medium (DMEM; Cellgro, MediaTek, Inc.), supplemented with 10% fetal bovine serum (FBS; HyClone), 1% penicillin–streptomycin, 1% sodium pyruvate (Cellgro, MediaTek, Inc.), 1% MEM nonessential amino acids (Sigma), and 1% L-glutamine. For imaging studies, cells were grown to confluence, passaged, and plated onto poly-D-lysine-coated plates. The plates, containing 2 mL of DMEM, were incubated at 37 °C with 5% CO_2 for at least 12 h. The media were removed, the cells were washed with 5 mL of PBS buffer, and solutions of the fluorescent probes in 2 mL of fresh DMEM were added. For all cell studies, the Cu^{II} complexes were generated in situ by combining a stock solution of the fluorescent sensor and $CuCl_2$ in a 1:1 molar ratio 1 h prior to addition to the cells. Plates were prepared with identical volumes from the same cell stock solution to provide an equal number of cells in each plate. For NO detection studies, NO production by iNOS was induced in Raw 264.7 murine macrophages with 1.6 μg/mL lipopolysaccharide (LPS; Sigma) and 495–4950 U/mL of recombinant mouse interferon-γ (IFN-γ; BD Biosciences). Cells were then incubated with 2.5 μM CuBRNO1 or 2.5 μM CuBRNO3 for 30 min. Then 5 μM HOECHST 33258 (Sigma) was added, and the cells were incubated for a further 30 min. Prior to imaging, cells were washed with 2 mL of PBS and then bathed with 1.5 mL of dye-free DMEM (Sigma). NO detection studies were performed by addition of 1.25 mM GSNO. For HNO imaging studies, HeLa and Raw 264.7 cells were treated as described above before addition of 1.25 mM Angeli's salt. Localization studies were performed in both HeLa and Raw 264.7 cells in the presence of 2.5 μM CuBRNO1 or 2.5 μM CuBRNO3 and 1.25 mM Angeli's salt. Prior to fluorescence imaging, the cells were incubated with either 3 μM ER-Tracker Blue Blue-White DPX (Invitrogen), 13 μM MitoTracker Green FM (Invitrogen), or CellLight Reagents BacMam 2.0 (Invitrogen) (10 parts per cell/16 h incubation) for 30 min.

Fluorescence Imaging. Fluorescence images were acquired on a Zeiss Axiovert 200 M inverted epifluorescence microscope equipped with an EM-CCD camera (Hamamatsu) and an X-Cite 120 metal halide lamp (EXFP). Differential interference contrast (DIC) and fluorescence images were obtained using an oil immersion 63× objective lens with exposure times ranging from 50 ms to 2 s. The microscope was operated with the *Volocity 6.01* software (Improvision), and images were analyzed with the *Volocity 6.01* software. All fluorescent images were deconvoluted and background-corrected. Images were measured before and after addition of Angeli's salt or NO-releasing agent. The image before addition of Angeli's salt or NO-releasing agent was taken as the background level.

RESULTS AND DISCUSSION

Design and Synthesis of Benzoresorufin-Based Sensors. An ongoing goal of our laboratory is the development of fluorescent sensors for NO and HNO. We found that an effective strategy for designing such species is to couple a metal-

dx.doi.org/10.1021/ic302793w | Inorg. Chem. 2013, 52, 3285–3294

Scheme 2. Synthetic Scheme for the Synthesis of Benzoresorufin-Based Sensors BRNO1−3

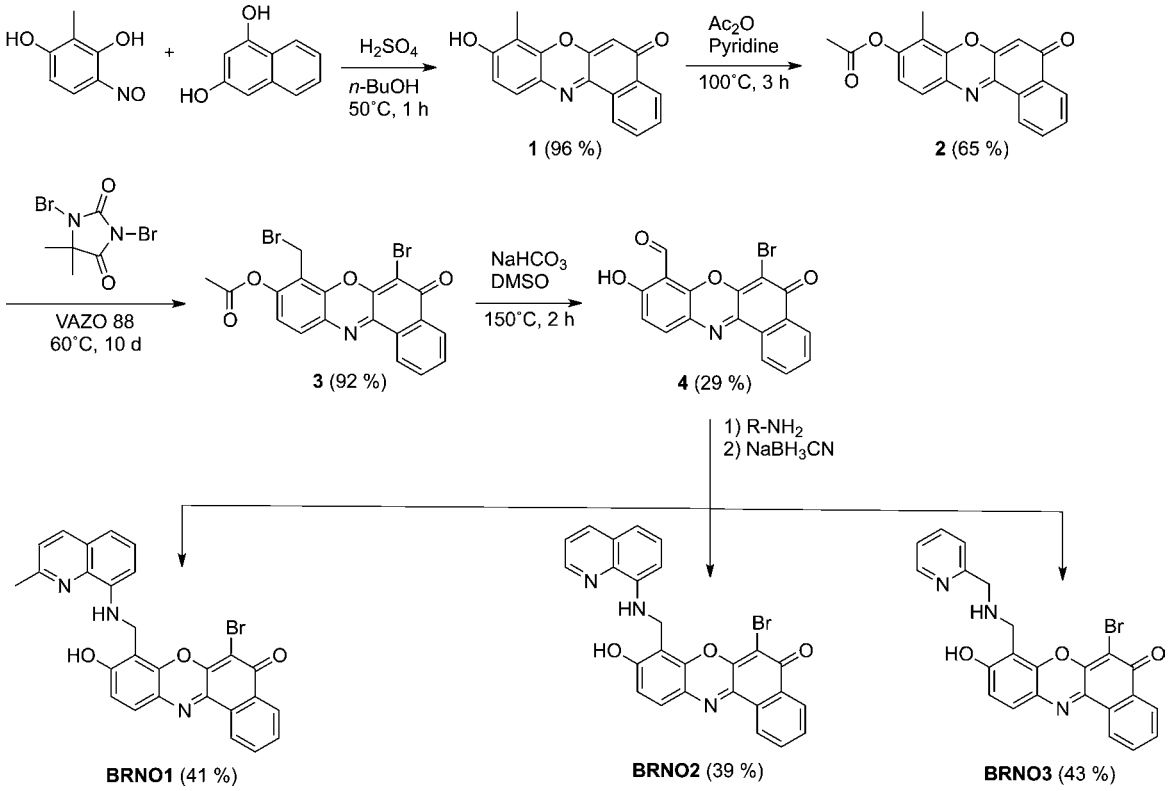

binding site with a fluorophore.[50] In the "off" state of the sensor, a paramagnetic ion in the metal-binding site quenches the emission of the fluorescent reporter by photoinduced electron transfer (PET). Upon reaction with NO, the paramagnetic ion is reduced, displaced, or both, thus eliminating the PET quenching pathway and triggering an emission turn-on response.[32,35,51−54] Our most successful NO sensors, which operate nicely in cellular environments, contain a 2-methyl-8-aminoquinoline metal-binding site and either a fluorescein (FL series) or a seminaphthofluorescein (SNFL series) dye as fluorescent reporters.[27−30] Cu^{II} is used as the paramagnetic fluorescence quencher. The methyl group in the 2 position of the aminoquinoline gives rise to only moderate Cu^{II}-binding affinities, characterized by K_d values of approximately 1.5 μM. In this study, we sought to change both the fluorescent reporter and metal-binding site. Benzoresorufin, which emits in the red, was chosen as the fluorophore, and in addition to our standard 2-methyl-8-aminoquinoline Cu^{II}-binding site, we investigated 8-aminoquinoline and 2-(methylamino)pyridine.

The overall synthetic strategy for preparing the desired benzoresorufin-based sensors is shown in Scheme 2. This synthetic approach is general and therefore offers a viable pathway to a wide variety of monofunctionalized benzoresorufin dyes. Following a similar procedure for the synthesis of naphthophenoxazones,[55] the reaction of 2-methyl-4-nitroresorcinol[37] and 1,3-dihydroxynaphthalene afforded **1**, which is readily purified in high yield by formation of the acetyl ester derivative **2**. The molecular structure of this compound, as determined by single-crystal X-ray diffraction, is presented in Figure S1 in the SI. To enable functionalization of the benzoresorufin moiety, we sought to selectively brominate the benzylic position. The bromination of compound **2** was carried out with 1,3-dibromo-5,5′-dimethylhydantoin and VAZO88, yielding dibrominated species **3** in high yield. The position of the two bromine atoms was unambiguously verified by single-crystal X-ray analysis (Figure S2 in the SI). The formation of **3** from **2** was monitored by ^{1}H NMR spectroscopy, revealing that bromination occurs first on the quinoid position, thus preventing isolation of a singly brominated species (Figure S3 in the SI). Because the exocyclic nitrogen atoms of aminoquinolines are only weak nucleophiles, the direct S_N2 reaction on bromide of **3** with 8-aminoquinolines was not a viable pathway to the target molecule. An alternative approach of reductive amination was therefore sought, involving oxidation of dibromide **3** to aldehyde **4**. This aldehyde is a versatile intermediate that may be used for functionalization of the dyes with a variety of metal-binding sites, thus allowing fine-tuning of the metal-binding properties and the electronic properties of the sensors. Three different sensors with varying metal-binding sites were synthesized by reductive amination. In all cases, a Schiff-base adduct was initially formed by reaction of aldehyde **4** with 2-methyl-8-aminoquinoline, 8-aminoquinoline, or 2-(aminomethyl)pyridine followed by reduction with sodium cyanoborohydride to afford the benzoresorufin-based dyes BRNO1, BRNO2, and BRNO3, respectively, in modest yield. For the more nucleophilic 2-(aminomethyl)pyridine, direct substitution of the benzylic bromine in **3** could be achieved in methanol with potassium carbonate as the base, affording BRNO3 with yield similar to that of the two-step route.

Photophysical Properties. The photophysical properties of BRNO1−3 were investigated in 50 mM PIPES buffer (100 mM KCl, pH 7) to reflect physiological conditions. The results are summarized in Table 1. At pH 7, BRNO1 and BRNO2 exhibit a very broad band in their absorption spectra, with a maximum at 470 nm and a lower-energy shoulder at 570 nm.

dx.doi.org/10.1021/ic302793w | Inorg. Chem. 2013, 52, 3285−3294

Table 1. Photophysical Properties of the BRNO Derivatives

	BRNO1	BRNO2	BRNO3
absorption			
λ_{max} (nm), ε (M^{-1} cm^{-1})	470, 5590 ± 300	470, 4390 ± 570	470, 5030 ± 630
	570, 2280 ± 230	570, 2160 ± 210	563, 11900 ± 1100
emission			
λ_{max} (nm), Φ (%)	623, 5.5 ± 0.2	623, 4.8 ± 0.4	625, 25 ± 4
brightness			
($\Phi\varepsilon$, M^{-1} cm^{-1})	125	103	2974
acid/base constants			
$pK_{a,1}$	6.46 ± 0.05	6.49 ± 0.03	5.93 ± 0.05
$pK_{a,2}$	9.57 ± 0.14	9.75 ± 0.15	10.29 ± 0.37

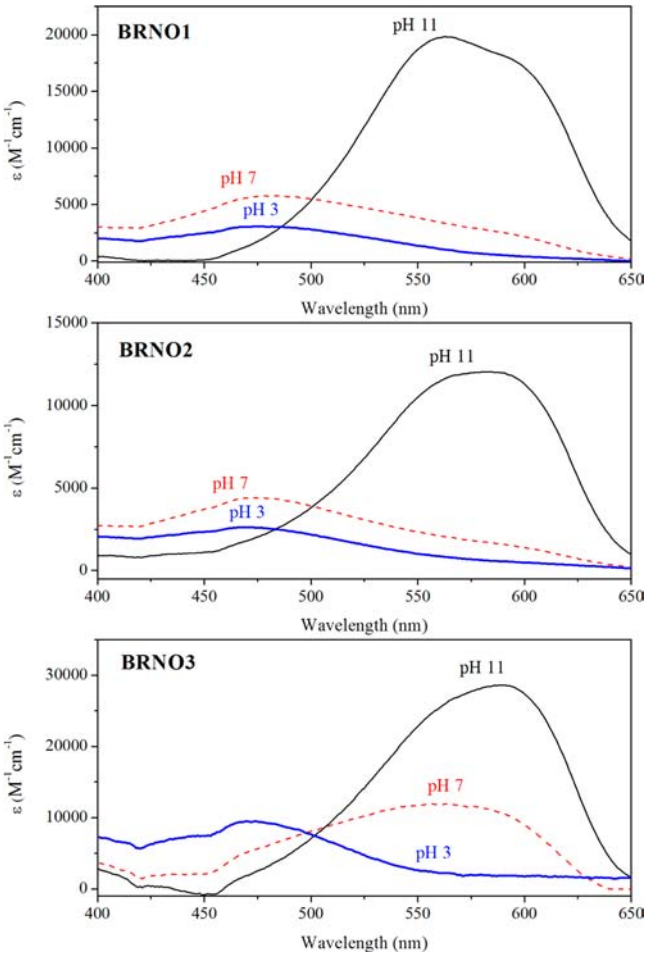

Figure 1. UV–vis absorption spectra of BRNO1 (top), BRNO2 (center), and BRNO3 (bottom) at different pH values.

The extinction coefficients for the 470 nm maximum are only 5590 M^{-1} cm^{-1} for BRNO1 and 4390 M^{-1} cm^{-1} for BRNO2. In contrast, the absorption spectrum of the 2-(aminomethyl)-pyridine derivative BRNO3 is marked by a lower-energy band centered at 563 nm of greater intensity (ε_{563} = 11900 M^{-1} cm^{-1}; Figure 1). Upon excitation of BRNO1 and BRNO2 at 570 nm, a weak emission band (ϕ_{BRNO1} = 0.055 ± 0.002; ϕ_{BRNO2} = 0.048 ± 0.004) is observed at 625 nm. These low luminescence quantum yields are similar to those reported for previously described NO sensors FL1 (ϕ = 0.077 ± 0.002)[27] and SNFL1 (ϕ = 0.027 ± 0.004)[30] and suggest a common quenching effect caused by the nitrogen lone pair of the amine in the metal-binding group. BRNO3, on the other hand, exhibits stronger emission. Upon excitation at 563 nm, an emission band at 625 nm is observed, and the photoluminescence quantum yield is 0.25. The significantly higher quantum yield and extinction coefficient of BRNO3 in comparison to the other derivatives demonstrate that the metal-binding site can modify the electronic properties of the ground and excited states of the dye. This observation suggests that modifying the metal-binding sites of metal-based sensors is a viable strategy for adjusting not only the binding affinity but also the photophysical properties of the system.

As for the fluorescein-based FL dyes, the absorbance and emission spectra of BRNO1–3 are sensitive to changes in pH because of the proton-accepting properties of the metal-binding sites and the dye itself. The pH dependence of the absorbance and emission properties of the metal-free dyes was therefore investigated. Under basic conditions (pH 11), the three compounds all display a strong broad absorbance feature between 550 and 610 nm. This band, presumably arising from the deprotonated sensors, is more intense than those observed at pH 7. At low pH values, the absorption decays with concomitant formation of a weaker feature centered at 470 nm (Figure 1). The emission properties of the fluorophores also vary with pH. Maximum emission intensity was observed between pH 7.5 and 9.5 for BRNO1 and BRNO2, whereas for BRNO3, maximum emission occurs between pH 7.0 and 9.0. The slightly different ranges for the maximum emission intensity of the aminoquinoline-based (BRNO1 and BRNO2) and (aminomethyl)pyridine-based (BRNO3) sensors most likely reflect disparate pK_a values associated with the different metal-binding sites. Analysis of the integrated emission data as a function of pH returned apparent pK_a values of 6.5 and 9.6 for BRNO1, 6.5 and 9.7 for BRNO2, and 5.9 and 9.6 for BRNO3 (Figure 2 and Table 1). These values are significantly higher

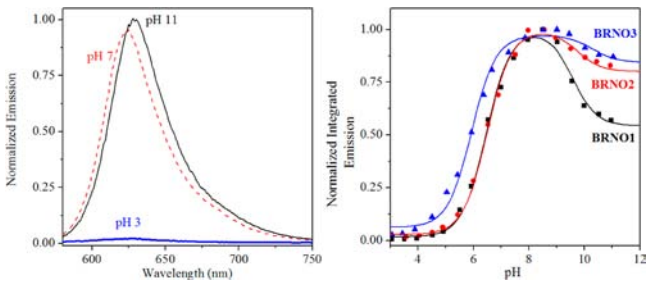

Figure 2. Fluorescence spectrum of BRNO3 at different pH values (left) and the pH dependence of the fluorescence intensity (right).

than the pK_a values reported for SNFL1 (4.9, 6.3, and 7.5),[30] indicating that the benzoresorufin confers a higher degree of basicitity to the molecules. The pH-dependent emission properties of the compounds reveal that all dyes described here exhibit high fluorescence under physiological conditions, with less than a 10% change in fluorescence within 2 pH units from pH 7.

DFT Calculations. To gain insight into the pH-dependent photophysical properties of BRNO1–3, DFT calculations were employed. Because BRNO1 and BRNO2 contain similar aminoquinoline metal-binding sites, DFT calculations were only carried out for BRNO1 and BRNO3 to compare how their different metal-binding groups affect the properties of the sensors. The geometries of BRNO1 and BRNO3, in both

dx.doi.org/10.1021/ic302793w | Inorg. Chem. 2013, 52, 3285–3294

neutral protonated and anionic deprotonated forms, were optimized in the gas phase at the B3LYP/6-31g(d,p) level of theory. Using these geometries, TDDFT calculations with an implicit water solvation model were employed to simulate the UV−vis absorbance spectra and to investigate the nature of the corresponding excited states. For the deprotonated anionic form of BRNO1, a transition (S_2) having a large oscillator strength (f = 0.736) is predicted at 528 nm. This calculated transition energy is 0.12 eV (30 nm) greater than that of the experimentally observed absorbance, which has a maximum at 560 nm (Figure S4 in the SI). An EDDM depicting the charge redistribution in this excited state is shown in Figure 3, where

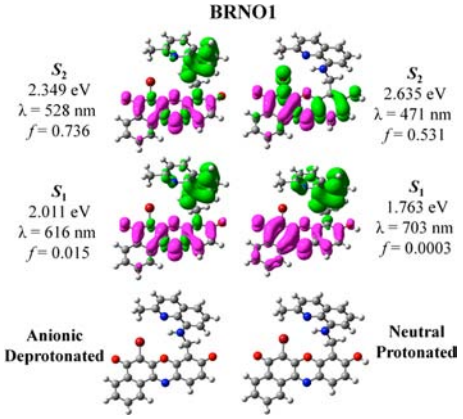

Figure 3. EDDMs of the two lowest-energy singlet excited states of BRNO1 in both the anionic deprotonated (left) and neutral protonated (right) forms. Green lobes represent holes, whereas purple lobes are electrons.

green lobes correspond to holes and purple lobes to electrons. On the basis of the EDDM, the excited state is assigned to a mixed transition with components of both benzoresorufin $\pi-\pi^*$ and aminoquinoline-to-benzoresorufin ligand-to-ligand charge transfer (LLCT) character. The mixture of LLCT into this excited state may give rise to the low observed emission quantum yield. The S_1 state of this deprotonated anion occurs at 616 nm with a low oscillator strength (f = 0.015). On the basis of its EDDM, the nature of the S_1 state is identical with that of the allowed S_2 state (Figure 3). For the neutral protonated form of BRNO1, the main allowed transition (S_2; f = 0.531) blue shifts relative to that of the deprotonated form, appearing at 471 nm. This calculation is in good agreement with the experimentally observed transition centered at 470 nm for BRNO1 measured at pH 3 in aqueous solutions (Figure S5 in the SI), The EDDM of this excited state reveals it to be primarily benzoresorufin $\pi-\pi^*$ in character. The S_1 excited state of the protonated species exhibits a low oscillator strength (f = 0.0003) and is therefore not expected to be an allowed transition. The EDDM (Figure 3) of the S_1 state indicates that it corresponds to an aminoquinoline-to-benzoresorufin LLCT. This dark charge-transfer excited state provides a plausible nonradiative decay pathway for the $\pi-\pi^*$ S_2 state. This hypothesis is consistent with the significant decrease in emission intensity of BRNO1 observed upon adjustment of the solution pH from 11 to 3 (Figure 2). The S_1 excited state of the deprotonated anionic form of BRNO3, which contains an (aminomethyl)pyridine metal-binding site, is computed to occur at 529 nm, with a large oscillator strength (f = 0.8182). This calculated value is 0.23 eV higher in energy than that measured experimentally from the absorbance spectrum of BRNO3 in pH 11 aqueous solution (Figure S6 in the SI). The EDDM of this excited state (Figure 4) reveals it to be a

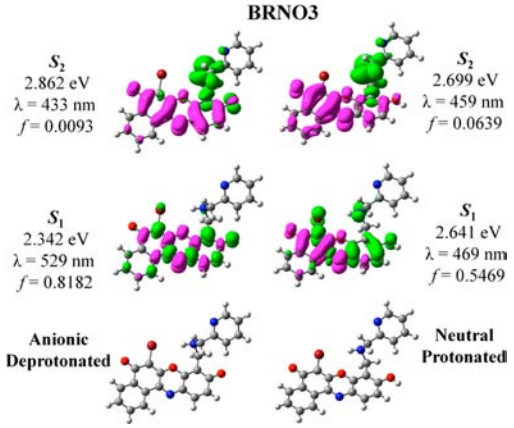

Figure 4. EDDMs of the two lowest-energy singlet excited states of BRNO3 in both the anionic deprotonated (left) and neutral protonated (right) forms. Green lobes represent holes, whereas purple lobes are electrons.

benzoresorufin $\pi-\pi^*$ transition. The pure $\pi-\pi^*$ character of the lowest-energy transition for BRNO3 is in contrast to the lowest-energy excited state of BRNO1, which is characterized in part as a LLCT. The lack of this charge transfer, which is expected to favor nonradiative emission, in the S_1 state of BRNO3 is consistent with the higher photoluminescent quantum yield of this sensor (Φ = 25%) compared to those of BRNO1. The large oscillator strength (f = 0.5469) of the S_1 state suggests that this transition is allowed, whereas the smaller oscillator strength (f = 0.0639) of S_2 indicates a smaller degree of allowed character. The S_1 and S_2 excited states of the neutral, protonated form of BRNO3 are separated by only 0.028 eV. The computed absorbance maximum of 469 nm is in good agreement with the value of 470 nm experimentally determined for BRNO3 at pH 3 in aqueous solution (Figure S7 in the SI). The nature of the S_1 and S_2 excited states is given by their EDDMs, shown in Figure 4. The S_1 state is primarily a benzoresorufin $\pi-\pi^*$ transition, whereas the S_2 state originates from charge transfer from the amine lone pair to the benzoresorufin π^* orbital (n−π^*). Of these two excited states, only the S_1 state is expected to be emissive because it involves only the fluorescent benzoresorufin unit. The small energy difference (0.058 eV) between the emissive S_1 and dark S_2 states renders these two states thermally accessible at room temperature (k_BT = 0.0256 eV at 25 °C). Therefore, the significant emission quenching at low pH of BRNO3 (Figure 2) arises from thermal population of the dark S_2 state. At higher pH values, where BRNO3 is largely deprotonated, the nonemissive S_2 state (Figure 4) lies 0.52 eV above the S_1 state and is not accessible at room temperature.

Metal-Binding Properties. Metal ions are endogenous to biological systems and can potentially interact with and influence the emissive properties of metal-based sensors. We therefore investigated the emission response of BRNO1−3 in the presence of several such metal ions. Upon addition of 1000 equiv of alkali or alkaline-earth metals, no significant change in fluorescence intensity was observed for all three dyes (Figure 5). When late-first-row transition metals were added, a small decrease of fluorescence intensity was observed. The largest

dx.doi.org/10.1021/ic302793w | Inorg. Chem. 2013, 52, 3285−3294

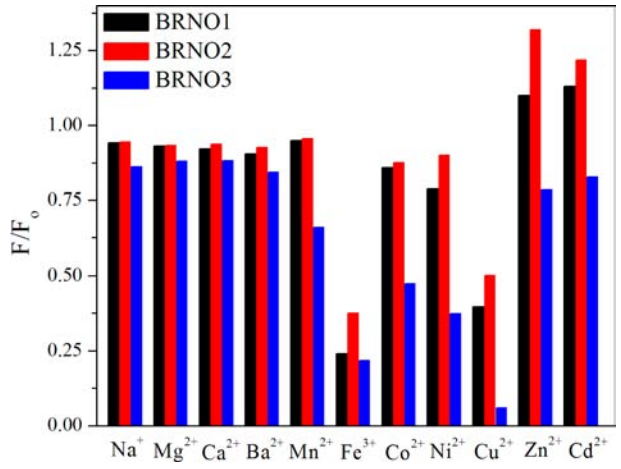

Figure 5. Fluorescence response (F/F_0) of the BRNO sensors upon addition of 1000 equiv of metal ions.

decrease in emission intensity occurred following addition of Cu^{2+} or Fe^{3+}. Addition of the diamagnetic metal ions, Zn^{2+} and Cd^{2+}, induced small increases in the emission of BRNO1 and BRNO2, whereas BRNO3 displayed a slight decrease in emission. The small response of the BRNO sensors to Zn^{2+} is somewhat surprising because analogous monotopic fluorescein-based derivatives (QZ1) exhibit a 42-fold turn-on upon Zn^{2+} addition.[56] For fluorescein-based zinc sensors, the zinc ion serves to lower the energy of the nitrogen lone pairs in the metal-binding sites, thereby inhibiting them from quenching the fluorescence by a PET mechanism.[57] The DFT calculations presented above are consistent with the inability of the BRNO sensors to turn-on with Zn^{2+}. For BRNO1 and BRNO2, the effect of zinc coordination on the energy of the the nitrogen lone pair would have little impact on quenching charge transfer from the aromatic π orbitals of the quinoline that is predicted for the S_1 and S_2 excited states. For BRNO3 in the deprotonated anionic form, the n–π* transition is significantly higher in energy than the emissive benzoresorufin π–π* and therefore unable to quench emission, even in the metal-free form. The lack of a turn-on response upon interaction with Zn^{2+} is an advantageous property of these sensors over first-generation analogues because no false-positive response of the sensors to highly abundant endogenous Zn^{2+} will occur.

Previously reported NO and HNO sensors utilize the Cu^{2+}/Cu^{+} redox couple to modulate the fluorescence response. In the 2+ oxidation state, the paramagnetic copper ion quenches the emission of the fluorophore.[27,33] Upon reduction of the copper ion to the diamagnetic 1+ oxidation state by NO or HNO, the emission is restored. To investigate the viability of this sensing mechanism for the BRNO compounds, more detailed metal-binding and photophysical studies were carried out in the presence of Cu^{2+}. Titration of the sensors with $CuCl_2$ revealed a 1:1 binding stoichiometry (Figure S8 in the SI). Addition of 1 equiv of $CuCl_2$ resulted in a decrease in fluorescence intensity (Figure S8 in the SI), from which the Cu^{2+} dissociation constants (K_d) were determined by emission titrations as 4470 ± 50 (BRNO1), 400 ± 60 (BRNO2), and 18 ± 2 nM (BRNO3) (Figures S9 and S10 in the SI). These values are consistent with the nature of the different metal-binding sites in the three sensors. The chelating groups of BRNO1 and BRNO2 differ only by the presence, in BRNO1, of a methyl group ortho to the nitrogen atom of the quinoline ring in BRNO2. This methyl group presumably destabilizes Cu^{2+} binding due to steric crowding. This destabilization is reflected by a dissociation constant of BRNO1 that is 1 order of magnitude higher than that of BRNO2. BRNO3, with its 2-(aminomethyl)pyridine group, binds Cu^{2+} most effectively. The dissociation constant of the Cu^{2+}-BRNO3 complex is more than 1 order of magnitude smaller than that of BRNO2. The larger Cu^{2+} affinity of BRNO3 may arise from the greater flexibility as well as the higher basicity of the secondary nitrogen atom of the 2-(aminomethyl)pyridine unit by comparison to the more rigid aminoquinoline metal-binding sites in the other two sensors.

Reactivity with ROS and RNS. The response of our copper-based sensors (CuBRNO1–3), assembled by treatment of BRNO1–3 with 1 equiv of $CuCl_2$ under anaerobic conditions, to different RNS and ROS was investigated. The CuBRNO probes were treated with 500 equiv of the RNS or ROS, and the emission response was recorded after 60 min (Figure 6). The reaction with the oxidizing agents sodium

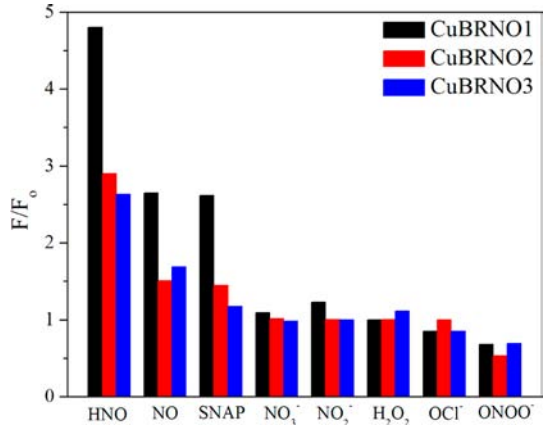

Figure 6. Comparison of the selectivity for RNS/ROS for $[CuBRNO1]^+$, $[CuBRNO2]^+$, and $[CuBRNO3]^+$ in 50 mM PIPES buffer (100 mM KCl, pH 7, 37 °C, 60 min) after addition of 500 equiv of RNS/ROS. Excitation wavelength: 570 nm, BRNO1 and BRNO2; 563 nm, BRNO3. integrated fluorescence emission from 590 to 800 nm.

hypochlorite and hydrogen peroxide induced no significant change in emission for any of the three sensors. Peroxynitrite, a strong oxidant, decreases the emission, probably owing to the formation of nonfluorescent oxidized resazurin derivatives. Unexpectedly, the reaction with NO only led to 2.6- (BRNO1), 1.5- (BRNO2), and 1.7-fold (BRNO3) fluorescence increases. A similar response was observed when the NO-releasing SNAP was added. Addition of Angeli's salt, $Na_2N_2O_3$, an HNO source, generated a larger turn-on response, with a 4.8-fold increase in fluorescence intensity for CuBRNO1. Angeli's salt decomposes in aqueous solutions to release HNO and nitrite ions.[58] To verify that nitrite was not causing the increase in emission, this ion was added to the probes. No increase in fluorescence was observed, proving that HNO rather than NO_2^- gives rise to the turn-on response. On the basis of emission, these probes are more effective for sensing HNO than NO. Furthermore, they exhibit selectivity over other ROS and RNS tested here. Because Fe^{3+}, like Cu^{2+}, quenches the emission of the BRNO sensors, we investigated the response of the Fe^{III}BRNO complexes to ROS and RNS. These studies revealed little

dx.doi.org/10.1021/ic302793w | Inorg. Chem. 2013, 52, 3285–3294

utility of the Fe^{III}BRNO system for sensing RNS and ROS (Figure S11 in the SI).

Mechanism of HNO and NO Sensing. We previously reported mechanistic investigations for a related NO-sensing probe, CuFL1, which utilizes a 2-methyl-8-aminoquinoline Cu^{2+}-binding site like that in BRNO1 but with fluorescein as the fluorophore.[35] The reaction of CuFL1 with NO reduces copper from the 2+ to 1+ oxidation state, forming an N-nitrosated fluorescein derivative, FL1-NO, in the process. In contrast to FL1 and CuFL1, FL1-NO is highly fluorescent. The sensing mechanism of our previously reported HNO sensor, CuBOT1, has also been investigated.[33] Although this compound does not react with NO, HNO reduces the emission-quenching paramagnetic Cu^{II} ion and induces a turn-on response. As in these previous studies, we sought to investigate the mechanisms by which CuBRNO1 responds to both NO and HNO.

The reaction of BRNO1 with 1 equiv of $CuCl_2$ decreases the emission intensity to one-fifth of its original value, most likely due to quenching effect of the photoexcited state by the paramagnetic Cu^{II} ion. An ESI-MS spectrum of freshly prepared CuBRNO1 shows the molecular ion peak of $[Cu^{II}BRNO]^+$ at m/z 573.1 (calcd m/z 573.0). Addition of NO or SNAP to CuBRNO1 induces a 2.6-fold emission turn-on, and the ESI-MS spectrum revealed the presence of a molecular ion peak at m/z 538.9, corresponding to the N-nitrosated species BRNO1-NO (calcd m/z 539.0 for $[BRNO1 + NO - H]^+$). Reaction of $NOBF_4$ with BRNO1 in acetonitrile afforded BRNO1-NO, as evidenced by the same molecular ion peak in the ESI-MS spectrum. Treatment of BRNO1 with NO gas in the absence of copper, on the other hand, gave no reaction, thereby demonstrating the importance of the Cu^{II} ion as an electron acceptor. An aliquot from the reaction mixture of $NOBF_4$ and BRNO1 in MeCN was diluted into PIPES buffer after 1 h, and the emission spectrum was recorded. Unexpectedly, a 1.8-fold decrease in fluorescence intensity compared to that of BRNO1 was observed (Figure S12 in the SI). Therefore, in contrast to FL1-NO and FL1, BRNO1-NO is less emissive than BRNO1. The relative order of emission intensity is BRNO1 > BRNO1-NO > CuBRNO1. The low observed turn-on response induced upon treatment of CuBRNO1 with NO is therefore a consequence of the intrinsically low emission intensity of BRNO1-NO. This result is not predicted by TDDFT calculations. The lowest-energy singlet excited state of BRNO1-NO is a benzoresorufin $\pi-\pi^*$ transition with a large oscillator strength of 0.701 (Figure S13 in the SI). The lack of charge-transfer character in this excited state suggests that it should be highly emissive, or at least more so than BRNO1. Therefore, additional nonradiative decay pathways must operate in BRNO1-NO. Decay by internal conversion, perhaps through the newly introduced NNO vibrational mode, is one possible explanation.

As discussed above, treatment of CuBRNO1 with Angeli's salt as an HNO source induces a 4.8-fold increase in emission after 2 min (Figure S14 in the SI). This 4.8-fold turn-on effectively corresponds to restoration of the fluorescence of copper-free BRNO1 because removal of copper from CuBRNO1 with ethylenediaminetetraacetic acid generates the same response. After the 4.8-fold turn-on, subsequent additions of Angeli's salt produced no further increases in emission intensity. Additionally, the emission properties of copper-free BRNO1 do not change in response to Angeli's salt. By analogy to the mechanism of HNO sensing for CuBOT1,[33] we hypothesized that HNO reduces the paramagnetic Cu^{II} center in CuBRNO1 to restore the emission of BRNO1. To investigate this possibility, the reaction of CuBRNO1 with Angeli's salt was monitored by EPR spectroscopy. For CuBRNO1, an axial signal is observed in the EPR spectrum due to the $S = {}^1/_2$ Cu^{II} ion (Figure S15 in the SI). Addition of Angeli's salt to this solution led to the disappearance of this signal (Figure S15 in the SI). This observation is consistent with reduction of Cu^{II} by HNO to form a diamagnetic, EPR-silent Cu^{I} ion. Although this EPR study verifies that Cu^{II} is reduced by HNO, it does not establish whether the newly formed Cu^{I} ion remains bound and whether or not this ion can affect the photophysical properties of the sensor. An ESI-MS spectrum of the reduced EPR solution revealed only the presence of free BRNO1, suggesting that reduction of copper leads to its dissociation. A 1:1 mixture of the Cu^{I} source $[Cu(CH_3CN)_4]PF_6$ and BRNO1 in acetonitrile, however, does show evidence for the formation of a Cu^{I} complex judging by the observation of a molecular ion peak corresponding to $[CuBRNO + H]^+$ in the ESI-MS spectrum (m/z 575.9; calcd m/z 576.0). The fluorescence spectrum of this mixture in aqueous buffer does not show Cu^{I}-induced changes in the emission intensity of BRNO1. Therefore, the Cu^{I} ion either does not bind strongly to BRNO1 or, if it does, it has little effect on the emission intensity, as for other diamagnetic metal ions tested (Figure 5).

Because the Cu^{II}/Cu^{I} redox couple is crucial for mediating the detection of HNO in this system, the electrochemical properties of CuBRNO1−3 were investigated by cyclic voltammetry in acetonitrile. Quasi-reversible reduction features occur at 90, 150, and 10 mV vs Fc/Fc^+ for CuBRNO1−3, respectively (Figure S16 in the SI). These values are close to that of the Cu^{II}/Cu^{I} couple of $CuCl_2$ under the same conditions (130 mV vs Fc/Fc^+). The reduction potential corresponding to the HNO/NO couple is −0.36 V in water.[59] In acetonitrile, conditions similar to those used for our copper complexes, NO is reduced irreversibly with an onset potential of approximately −1 V versus the Fc/Fc^+ couple. Therefore, all three sensors are thermodynamically capable of oxidizing HNO to NO. To confirm the formation of NO gas, EI-MS measurements were carried out on the headspace of a reaction mixture of CuBRNO1 and Angeli's salt. These measurements confirmed the formation of NO gas (Figure S17 in the SI), consistent with our hypothesis that HNO reduces the CuBRNO sensors.

NO and HNO Detection in Living Cells. Fluorescence imaging studies were carried out to investigate whether the CuBRNO sensors can detect NO and HNO in living cells, as they do in cuvettes. Only CuBRNO1 and CuBRNO3 were used for these studies because they contain significantly different metal-binding sites and were therefore expected to exhibit different intracellular properties. Human cervical cancer cells, HeLa, and murine macrophage cells, Raw 264.7, were investigated. The Raw 264.7 cells allow for stimulation of endogenous NO production by iNOS following treatment with LPS and INF-γ.[60] Treatment of both cell types with 2.5 μM CuBRNO1 or CuBRNO3 resulted only in negligible emission in the absence of an analyte. In contrast, treatment of both cell lines with 500 equiv of Angeli's salt in the presence of CuBRNO1 or CuBRNO3 produced a distinct enhancement in emission after 15 min of incubation (Figure 7). In all cases, the observed increase in emission was comparable to that found when similar experiments were performed in a cuvette, demonstrating the suitability of the sensors to detect HNO

dx.doi.org/10.1021/ic302793w | Inorg. Chem. 2013, 52, 3285−3294

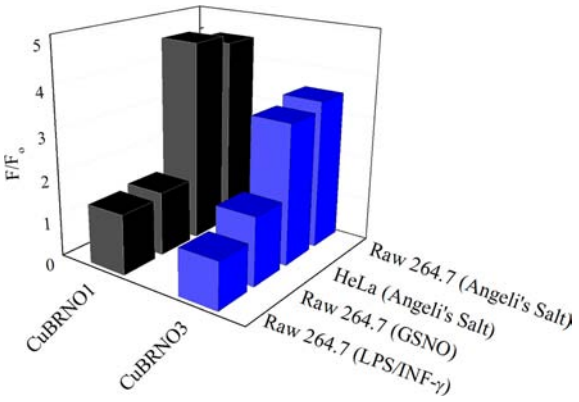

Figure 7. Quantified fluorescence turn-on in cells after treatment with Angeli's salt as well as NO-releasing GSNO and stimulation of iNOS by LPS/INF-γ in the presence of in situ generated $[CuBRNO1]^+$ and $[CuBRNO3]^+$.

in live cells. To assess their ability to detect intracellular NO, we induced NO production by iNOS in Raw 264.7 cells by adding LPS and INF-γ.[60] Raw 264.7 macrophages generate micromolar concentrations of NO following treatment with endotoxins and cytokines.[61] Accordingly, these cells are ideal for studying the response of NO probes to endogenously produced NO. After stimulation of NO production, 1.4- and 1.2-fold increases in emission intensity were observed for CuBRNO1 and CuBRNO3, respectively (Figure 7). As a control experiment, Raw 264.7 macrophages were treated with 500 equiv of GSNO. This experiment provides a direct comparison of the turn-on response of CuBRNO1 and CuBRNO2 induced by endogenous and exogenous NO sources within the same cell line. In agreement with our findings for endogenously produced NO, treatment of cells containing our sensors with GSNO resulted in a similar, small enhancement of emission for both sensors (Figure 7). Representative cell images are presented in Figures 8 and S18 in the SI. Colocalization experiments, performed with the sensor in the presence of Angeli's salt, indicated that

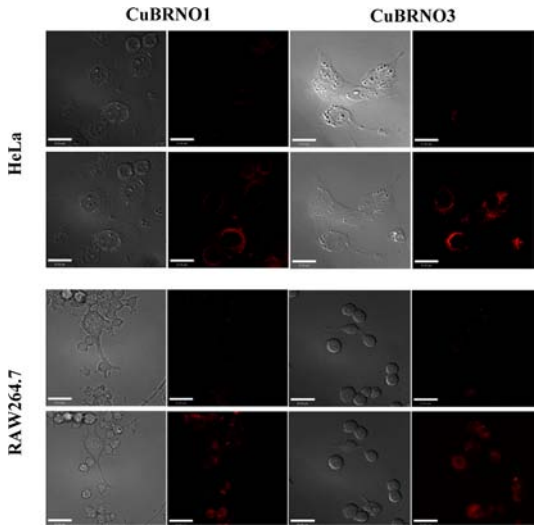

Figure 8. Fluorescence imaging of HNO in HeLa and Raw 264.7 cells. For each set, the top image corresponds to treatment of cells with the fluorescent probe. The bottom image corresponds to cells treated with Angeli's salt. (left) DIC images. (right) Fluorescence images. Scale bar = 25 μm.

both CuBRNO1 and CuBRNO3 localize to the endoplasmic reticulum (ER). The spatial emission overlap between the BRNO sensors and the ER tracker dye is marked by a Pearson correlation coefficient[62] of 0.61 for CuBRNO1 and 0.74 for CuBRNO3 (Figures S19 and S20 and Table S13 in the SI). This observation is in good agreement with literature reports that resorufin dyes localize in the ER.[63] In addition to the ER, a significant degree of membrane staining was observed.

CONCLUSION

We have presented three novel benzoresorufin-based NO and HNO fluorescent sensors. The use of benzoresorufin as the fluorophore gives rise to emission at 625 nm, a region favorable for biological imaging studies. In their copper-free forms, BRNO1 and BRNO2 exhibit only weak fluorescence. BRNO3, which contains a 2-(aminomethyl)pyridine metal-binding site, has a significantly higher photoluminescent quantum yield owing to the absence of low-energy charge-transfer excited states. In the Cu^{II}-bound form, these complexes serve as selective sensors for NO and HNO over other ROS and RNS with modest increases in emission intensity. The observation that higher turn-on responses for these sensors occur for HNO rather than NO is an unexpected result based on the structural similarities of the metal- and NO-reacting sites with respect to those in previously reported NO sensors in the FL and SNFL series. These results suggest that, in addition to the chemistry occurring at the metal-binding site, the energy levels of the fluorophore unit also play a significant role in modulating the emission response and must be considered carefully. Moreover, they indicate that a secondary amine in the copper-binding site is necessary but not sufficient for selectively sensing NO, whereas the best HNO sensor is obtained by blocking this secondary amine and further tuning the electronic properties. Mechanistic studies revealed that Cu^{II} reduction is necessary for both HNO or NO turn-on. The fluorescence turn-on observed with the Cu^{II}BRNO probes reveals that the redox potentials of the complexes are largely influenced by the fluorescent dye, which participates in metal coordination, and are only slightly influenced by the different amine chelating moieties. The metal-binding affinity influences fluorescence turn-on after addition of NO or HNO. There is a lower fluorescence turn-on for both HNO and NO with tighter binding of Cu^{II}. Despite the small turn-on response to NO, these sensors are quite effective at detecting NO and HNO in both the cuvette and living cells.

ASSOCIATED CONTENT

Supporting Information

NMR data of all compounds, as well as crystallographic data of compounds **2** and **3**, additional DFT results, Cu^{II}-binding studies, RNS/ROS studies with $[FeBRNO]^{2+}$, time dependency study of HNO turn-on, EPR data, cyclic voltammetry data, headspace EI-MS data, and intracellular localization experiments. This material is available free of charge via the Internet at http://pubs.acs.org.

AUTHOR INFORMATION

Corresponding Author

*E-mail: lippard@mit.edu.

Notes

The authors declare no competing financial interest.

■ ACKNOWLEDGMENTS

This work was supported the National Science Foundation (Grant CHE-0611944 to S.J.L.). Instrumentation in the MIT DCIF is maintained with funding from NIH Grant 1S10RR13886-01. U.-P.A. thanks the Alexander von Humboldt Foundation for a postdoctoral fellowship. J.J.W. is a grateful recipient of a David H. Koch Graduate Fellowship. Daniel J. Graham and Dr. Amit Majumdar are thanked for assistance with headspace EI-MS experiments and X-ray crystallography, respectively.

■ REFERENCES

(1) Darley-Usmar, V.; Halliwell, B. *Pharm. Res.* **1996**, *13*, 649.
(2) Palmer, R. M. J.; Ferrige, A. G.; Moncada, S. *Nature* **1987**, *327*, 524.
(3) Kroencke, K.-D.; Fehsel, K.; Kolb-Bachofen, V. *Clin. Exp. Immunol.* **1998**, *113*, 147.
(4) Hobbs, A. J.; Higgs, A.; Moncada, S. *Annu. Rev. Pharmacol. Toxicol.* **1999**, *39*, 191.
(5) Wang, Y.; Ruby, E. G. *Cell. Microbiol.* **2011**, *13*, 518.
(6) Tennyson, A. G.; Lippard, S. J. *Chem. Biol.* **2011**, *18*, 1211.
(7) Toledo, J. C.; Augusto, O. *Chem. Res. Toxicol.* **2012**, *25*, 975.
(8) Fukuto, J. M.; Carrington, S. J.; Tantillo, D. J.; Harrison, J. G.; Ignarro, L. J.; Freeman, B. A.; Chen, A.; Wink, D. A. *Chem. Res. Toxicol.* **2012**, *25*, 769.
(9) Marletta, M. A. *Cell* **1994**, *78*, 927.
(10) Muenzel, T.; Feil, R.; Muelsch, A.; Lohmann, S. M.; Hofmann, F.; Walter, U. *Circulation* **2003**, *108*, 2172.
(11) Moncada, S.; Higgs, E. A. *Br. J. Pharmacol.* **2006**, *147*, S193.
(12) Bult, H.; Boeckxstaens, G. E.; Pelckmans, P. A.; Jordaens, F. H.; Van Maercke, Y. M. *Nature* **1990**, *345*, 346.
(13) Butler, A. R.; Williams, D. L. H. *Chem. Soc. Rev.* **1993**, *22*, 233.
(14) Fukuto, J. M.; Dutton, A. S.; Houk, K. N. *ChemBioChem* **2005**, *6*, 612.
(15) Irvine, J. C.; Ritchie, R. H.; Favaloro, J. L.; Andrews, K. L.; Widdop, R. E.; Kemp-Harper, B. K. *Trends Pharmacol. Sci.* **2008**, *29*, 601.
(16) Feelisch, M. *Proc. Natl. Acad. Sci. U.S.A.* **2003**, *100*, 4978.
(17) Fukuto, J. M.; Chiang, K.; Hszieh, R.; Wong, P.; Chaudhuri, G. J. *Pharmacol. Exp. Ther.* **1992**, *263*, 546.
(18) Bermejo, S. E.; Saenz, D. A.; Alberto, F.; Rosenstein, R. E.; Bari, S. E.; Lazzari, M. A. *Thromb. Haemostasis* **2005**, *94*, 469.
(19) Miles, A. M.; Wink, D. A.; Cook, J. C.; Grisham, M. B. In *Methods in Enzymology*; Lester, P., Ed.; Academic Press: New York, 1996; Vol. *268*, p 105.
(20) Nagano, T.; Yoshimura, T. *Chem. Rev.* **2002**, *102*, 1235.
(21) Sasaki, E.; Kojima, H.; Nishimatsu, H.; Urano, Y.; Kikuchi, K.; Hirata, Y.; Nagano, T. J. *Am. Chem. Soc.* **2005**, *127*, 3684.
(22) Terai, T.; Urano, Y.; Izumi, S.; Kojima, H.; Nagano, T. *Chem. Commun.* **2012**, *48*, 2840.
(23) Yang, Y.; Seidlits, S. K.; Adams, M. M.; Lynch, V. M.; Schmidt, C. E.; Anslyn, E. V.; Shear, J. B. *J. Am. Chem. Soc.* **2010**, *132*, 13114.
(24) Dobmeier, K. P.; Riccio, D. A.; Schoenfisch, M. H. *Anal. Chem.* **2008**, *80*, 1247.
(25) Wong, P. S. Y.; Hyun, J.; Fukuto, J. M.; Shirota, F. N.; DeMaster, E. G.; Shoeman, D. W.; Nagasawa, H. T. *Biochemistry* **1998**, *37*, 5362.
(26) Reisz, J. A.; Zink, C. N.; King, S. B. *J. Am. Chem. Soc.* **2011**, *133*, 11675.
(27) Lim, M. H.; Xu, D.; Lippard, S. J. *Nat. Chem. Biol.* **2006**, *2*, 375.
(28) Lim, M. H.; Wong, B. A.; Pitcock, W. H.; Mokshagundam, D.; Baik, M.-H.; Lippard, S. J. *J. Am. Chem. Soc.* **2006**, *128*, 14364.
(29) McQuade, L. E.; Lippard, S. J. *Inorg. Chem.* **2010**, *49*, 7464.
(30) Pluth, M. D.; Chan, M. R.; McQuade, L. E.; Lippard, S. J. *Inorg. Chem.* **2011**, *50*, 9385.
(31) Tsuge, K.; DeRosa, F.; Lim, M. D.; Ford, P. C. *J. Am. Chem. Soc.* **2004**, *126*, 6564.
(32) Khin, C.; Lim, M. D.; Tsuge, K.; Iretskii, A.; Wu, G.; Ford, P. C. *Inorg. Chem.* **2007**, *46*, 9323.
(33) Rosenthal, J.; Lippard, S. J. *J. Am. Chem. Soc.* **2010**, *132*, 5536.
(34) Royzen, M.; Wilson, J. J.; Lippard, S. J. *J. Inorg. Biochem.* **2013**, *118*, 162.
(35) McQuade, L. E.; Pluth, M. D.; Lippard, S. J. *Inorg. Chem.* **2010**, *49*, 8025.
(36) Klein, C.; Batz, H.-G.; Hermann, R. U.S. Patent 4,954,630, 1990.
(37) Raphael, R. A.; Ravenscroft, P. *J. Chem. Soc., Perkin Trans.* **1988**, 1823.
(38) *APEX2 v2009*; Bruker AXS: Madison, WI, 2009.
(39) *SADABS: Area-Detector Absorption Correction*; University of Göttingen: Göttingen, Germany, 2001.
(40) Sheldrick, G. M. *Acta Crystallogr., Sect. A* **1990**, *46*, 467.
(41) Sheldrick, G. *Acta Crystallogr., Sect. A* **2008**, *64*, 112.
(42) *Gaussian 03*, revision D.01; Gaussian, Inc.: Wallingford, CT, 2004.
(43) Lee, C.; Yang, W.; Parr, R. G. *Phys. Rev. B* **1988**, *37*, 785.
(44) Becke, A. D. *J. Chem. Phys.* **1993**, *98*, 5648.
(45) Hehre, W. J.; Ditchfield, R.; Pople, J. A. *J. Chem. Phys.* **1972**, *56*, 2257.
(46) Cossi, M.; Rega, N.; Scalmani, G.; Barone, V. *J. Comput. Chem.* **2003**, *24*, 669.
(47) O'Boyle, N. M.; Tenderholt, A. L.; Lagner, K. M. *J. Comput. Chem.* **2008**, *29*, 839.
(48) Lim, M. D.; Lorkovic, I. M.; Ford, P. C. *Nitric Oxide*; Elsevier: San Diego, 2005; Vol. *396*, Part E, p 3.
(49) Bueno, C.; Villegas, M. L.; Bertolotti, S. G.; Previtali, C. M.; Neumann, M. G.; Encinas, M. V. *Photochem. Photobiol.* **2002**, *76*, 385.
(50) Tonzetich, Z. J.; McQuade, L. E.; Lippard, S. J. *Inorg. Chem.* **2010**, *49*, 6338.
(51) Sarma, M.; Kalita, A.; Kumar, P.; Singh, A.; Mondal, B. *J. Am. Chem. Soc* **2010**, *132*, 7846.
(52) Kalita, A.; Kumar, P.; Deka, R. C.; Mondal, B. *Inorg. Chem.* **2011**, *50*, 11868.
(53) Mondal, B.; Kumar, P.; Ghosh, P.; Kalita, A. *Chem. Commun.* **2011**, *47*, 2964.
(54) Sarma, M.; Mondal, B. *Inorg. Chem.* **2011**, *50*, 3206.
(55) Fischer, O.; Hepp, E. *Ber. Dtsch. Chem. Ges.* **1903**, *36*, 1807.
(56) Nolan, E. M.; Jaworski, J.; Okamoto, K.-I.; Hayashi, Y.; Sheng, M.; Lippard, S. J. *J. Am. Chem. Soc.* **2005**, *127*, 16812.
(57) Kowalczyk, T.; Lin, Z.; Voorhis, T. V. *J. Phys. Chem. A* **2010**, *114*, 10427.
(58) Dutton, A. S.; Fukuto, J. M.; Houk, K. N. *J. Am. Chem. Soc.* **2004**, *126*, 3795.
(59) Bartberger, M. D.; Liu, W.; Ford, E.; Miranda, K. M.; Switzer, C.; Fukuto, J. M.; Farmer, P. J.; Wink, D. A.; Houk, K. N. *Proc. Natl. Acad. Sci. U.S.A.* **2002**, *99*, 10958.
(60) Miwa, M.; Stuehr, D. J.; Marletta, M. A.; Wishnok, J. S.; Tannenbaum, S. R. *Carcinogenesis* **1987**, *8*, 955.
(61) Noda, T.; Amano, F. J. *Biochemistry* **1997**, *121*, 38.
(62) French, A. P.; Mills, S.; Swarup, R.; Bennet, M. J.; Pridmore, T. P. *Nat. Protocols* **2008**, *3*, 619.
(63) Hakamata, W.; Machida, A.; Oku, T.; Nishio, T. *Bioorg. Med. Chem. Lett.* **2011**, *21*, 3206.